Improved Monte Carlo techniques for the spectral synthesis of supernovae

L.B. Lucy[*]

ST-ECF, Karl-Schwarzschild-Strasse 2, D-85748 Garching bei München, Germany

Abstract. Improvements in Monte Carlo techniques for computing synthetic spectra of supernovae (SNe) are described and tested using a simplified model for the atmosphere of a Type Ia SN. In the first innovation, a procedure is implemented that replaces the previously-assumed line formation by resonance scattering with a branching model using Sobolev escape probabilities, and the resulting improvement is demonstrated by comparison with exact calculations for Fe II. In a second innovation, greatly accelerated convergence is achieved in the computation of emergent spectra by replacing the crude procedure of binning escaping Monte Carlo quanta with one based on the formal integral for emergent intensity. This is made possible by extracting line- and continuum source functions from a Monte Carlo simulation. Because of accelerated convergence, the required size of the Monte Carlo simulations is reduced by a factor ~ 300, thus greatly speeding up the calculation of model spectra and thereby allowing interactive diagnostic analyses of the spectra of newly-discovered SNe.

Key words: radiative transfer – methods: numerical – stars: atmospheres – stars: supernovae: general

1. Introduction

In two previous papers (Lucy 1987a, Paper I; Mazzali & Lucy 1993, Paper II), a Monte Carlo code for synthesizing the early-time spectra of SNe has been described. Originally written in the days following the explosion of SN 1987A and only modified slightly since, this code has become a standard diagnostic tool for analysing SNe spectra. Examples of SNe analyzed with this code are the following: SN 1987A (Lucy 1987b; Fosbury et al. 1987; Mazzali et al. 1992); SN 1990N (Mazzali et al. 1993); SN 1991T (Mazzali et al. 1995); SN 1991bg (Mazzali et al. 1997); SN 1993J (Zhang et al. 1995); and SN 1994D (Patat et al. 1996).

However, in the intervening decade, techniques of spectral synthesis have advanced significantly, and the available computer power has increased remarkably. The question therefore

Send offprint requests to: L.B. Lucy

[*] *Present address:* Astrophysics Group, Blackett Laboratory, Imperial College of Science, Technology and Medicine, Prince Consort Road, London SW7 2BZ

arises as to how this productive code should be upgraded. In seeking to answer this question, the prime consideration has been not to compromise the code's role as a diagnostic tool capable of being used interactively to make a rapid coarse analysis of the spectrum of a newly-discovered SN, thus allowing a quantitative astrophysical interpretation to replace the qualitative comparisons that traditionally suffice for an initial discovery paper. The code must therefore remain robust and fast. Accordingly, no attempt is made here to duplicate the level of physical sophistication incorporated, for example, in the code developed by Eastman & Pinto (1993).

A major simplifying assumption fundamental to the architecture of the previous code as well as to its predecessor stellar wind code (Abbott & Lucy 1985) is that of line formation by coherent scattering in the matter frame. In addition to lending itself naturally to a Monte Carlo treatment because of its elimination of photon splitting, this assumption has the further merit of automatically generating a radiation field that is rigorously divergence-free, thus incorporating this (almost exact) constraint even though the radiative equilibrium temperature distribution is not solved for.

In addition to these incidental benefits, treating every bound-bound transition as if it were a resonance line is more accurate than one might intuitively expect. When the constraint of statistical equilibrium is added to the constraints imposed by selection rules, the emissivity in a non-resonance line is often obliged not to differ greatly from the rate of absorption in that line (Chugai 1980; Abbott & Lucy 1985), thus restricting the fluorescent degradation of dilute radiation fields.

Nevertheless, improving the treatment of line formation should clearly be of high priority in updating the code. Accordingly, in the first of two innovations, a technique will be described that allows branching to occur after absorption by non-resonance transitions; and this is achieved with negligible impact on the complexity, speed or robustness of the Monte Carlo code. Moreover, the derived radiation field remains divergence-free.

The second aspect of the previous code that has been re-examined is the calculation of the emergent spectrum. Following standard Monte Carlo procedure, the synthetic spectrum provided by that code is derived from the photon packets that escape to infinity by binning them according to their rest fre-

quencies, with the result that Poisson noise is very evident unless one follows a huge number of packets. Interestingly, an almost noise-free emergent spectrum can be obtained even from a modest-sized Monte Carlo experiment by using the formal integral for the emergent intensity. This approach is made possible by first computing the source function implied by the Monte Carlo code's treatment of line formation. By reducing computer time, this second innovation greatly enhances the code's usefulness as an interactive diagnostic tool.

These two innovations are described and illustrated below in the context of computing SNe spectra. But they are equally relevant for stellar-wind codes and possibly also for other astrophysical problems.

2. Physical model

In this section, the assumptions that determine the structure of the supernova's envelope are stated. Here it should be emphasized that this aspect has been deliberately kept simple since this model serves only as a test-bed for the development of technique. In a companion paper, Mazzali (1999) will add the refinements described in Paper II and discuss the implications of the fully updated code for diagnostic studies of SNe spectra.

As in Papers I and II, a Schuster-Schwarzschild model is adopted for the line-forming region of a SN's envelope. Thus, at the lower boundary $r = R$, a black-body continuum is emitted, i.e.

$$I_\nu^+(R) = B_\nu(T_b) \tag{1}$$

where T_b, the boundary temperature, is to be determined. Bound-bound transitions in the region $r > R$ then impose a line spectrum on this featureless continuum.

In this investigation, the region $r > R$ is assumed to be isothermal both with respect to the characteristic temperature T_R of the ionizing continuum and to the local electron temperature T_e. Specifically, we set

$$T_e = T_R = 0.8T_b \tag{2}$$

The density at radius $r > R$ and elapsed time t is obtained from the assumption of homologous expansion and the specification of a reference model. Accordingly, we have

$$\rho(v,t) = \left(\frac{t_1}{t}\right)^3 \rho_1(v) \tag{3}$$

where $v = r/t$ is the constant velocity of the mass shell which is at radius r at time t, and $\rho_1(v)$ is the density-velocity profile at $t = t_1$. Here we use a single power-law approximation ($\rho \propto v^{-7}$) to the density plot given by Branch, Doggett & Thielemann (1985) for the Type Ia model W7 at $t_1 = 16$ days.

The treatment of excitation is that of Abbott & Lucy (1985). Thus, for normal levels,

$$\frac{n_i}{n_1} = W\frac{g_i}{g_1}e^{-\epsilon_i/kT_R} \tag{4}$$

where the dilution factor is simply set equal to its value in the optically-thin limit, i.e.

$$W = \frac{1}{2}\left[1 - \sqrt{1 - \left(\frac{R}{r}\right)^2}\right] \tag{5}$$

However, for metastable levels, we set $W = 1$, since the depopulation of these levels by upward transitions is also $\propto W$.

The adopted ionization formula is

$$\begin{aligned}\frac{N_{J+1}}{N_J}N_e &= \eta W\frac{2U_{J+1}}{U_J}\frac{(2\pi m_e kT_R)^{3/2}}{h^3}\\ &\times \left(\frac{T_e}{T_R}\right)^{1/2}e^{-\chi/kT_R}\end{aligned} \tag{6}$$

where

$$\eta = \zeta + W(1 - \zeta) \tag{7}$$

and ζ is the fraction of recombinations going directly to the ground state.

The correction factor η modifies Strömgren's (1939) treatment of nebular ionization to allow for ionization from excited states in circumstances where dilution is not extreme. Specifically, Eq. (6) is derived under the assumption that the ionizing continuum is dilute Wien, that photoionization coefficients are $\propto \nu^{-2}$, and that excited states have populations depleted by the factor W from Boltzmann at $T = T_R$. This formula was developed in the context of a collaboration with D.C. Abbott and was described and used in Paper I and also by Abbott in his work on SN 1987A (Schmutz et al. 1990). Further elaborations in the treatment of ionization described in Paper II are not included here.

The partition functions U_J needed for Eq. (6) are computed using the above excitation model – i.e., LTE partition functions are not assumed.

The chemical elements included in this model and their mass fractions are: C (0.01), O (0.01), Ne (0.01), Mg (0.01), Si (0.45), S (0.35), Ar (0.04), Ca (0.03), Fe (0.07), Co (0.01), and Ni (0.01). These crudely represent the abundances in model W7 of Nomoto et al. (1984) at or near the photosphere at maximum light. In this test-bed model, the abundances are assumed uniform throughout the atmosphere. However, in fitting observed spectra or in calculating spectra for explosion models, abundance stratification must be allowed for. This is of course a straightforward generalization of this code.

The basic parameters of this model are t, the elapsed time since explosion, the photospheric radius R (or, equivalently, the photospheric velocity $v_{ph} = R/t$), the bolometric luminosity L_{bol}, the reference density function $\rho_1(v)$, and the chemical composition.

A useful option introduced into this code is to drop L_{bol} as parameter and instead use $L(\lambda_1, \lambda_2)$, the luminosity in the wavelength interval (λ_1, λ_2). This is obviously more convenient when analysing an observed spectrum.

3. Line lists

In Papers I and II, atomic transitions and their gf-values were from Abbott (1982) and Kurucz & Peytremann (1975). In this work, these data have been replaced by the data on a CD-ROM distributed by Kurucz & Bell (1995). This data is manipulated as described below. In particular, in contrast to the previous stellar wind and supernova codes, the present code's improved treatment of line formation is greatly facilitated by creating *two* line lists containing identical data but differently ordered.

The first step in using the Kurucz-Bell data is to infer their atomic model for each ion. Thus, a file (I) is constructed in which, for each ion, the energy levels E_i featuring in the transition array and their J-values are tabulated. A second file (II) can then be constructed in which, for each ion, its transitions' $\log gf$ values are tabulated, with the transitions being identified *only* by u and l, the indices in file I of the upper and lower energy levels. These two files provide compact storage of the data and allow rapid construction of working line lists for specific models.

Because of the difference in the excitation formula (Sect. 2) between normal and metastable levels, it is useful to identify metastable levels in these files. This is done by replacing E_i by $-E_i$ in file I and l by $-l$ in file II.

From these basic files, a list of transitions relevant for a particular model is created as follows:

1) All lines of an element are excluded if it is absent from the adopted mixture.
2) All lines of an element's $(J + 1)$-th ion are excluded if $\chi_{J,J+1} > \chi_L$, an appropriate limiting potential.
3) Of the surviving transitions, a further culling eliminates all those with Sobolev optical depths everywhere $< \tau_L$, an appropriately small cut-off value.

Having thus excluded all inconsequential transitions, those that survive are organized into two line lists as follows:

I) Line list A: lines ordered according to frequency with $\nu_{k+1} \leq \nu_k$.
II) Line list B: lines grouped according to ion and then, for each ion, according to the index u of the transitions' upper levels.

Because of the expansion of the SN's envelope, the co-moving frequency of a photon in free flight decreases with time. Line list A serves therefore as usual to identify efficiently the next transition with which a photon (or photon packet) might interact. On the other hand, after a packet has been absorbed by the transition $l \to u$, the possible radiative decays are the set of permitted transitions $u \to i \, (< u)$ with the same upper level. But these transitions are contiguous in line list B, and so an appropriate random selection of the re-emitted packet's frequency can be simply and efficiently made.

4. Monte Carlo procedures

In Papers I and II, rather complete details are given of how the Monte Carlo calculation proceeds in the presence of electron- and resonance-line scattering. This section is therefore restricted to the changes required by the improved treatment of line formation and to the development of a Monte Carlo estimator required when calculating the emergent spectrum from the formal integral.

4.1. Branching

As in the previous codes, the basic quanta in this Monte Carlo calculation are packets of identical photons, so that $\epsilon(\nu) = nh\nu$ is the energy of a packet containing n photons. In a single Monte Carlo experiment, N packets of energy $\epsilon(\nu) = \epsilon_0$ are launched across the lower boundary $r = R$ and their complicated trajectories through the expanding envelope followed as before. But now, when a packet is absorbed by the transition $l \to u$, we no longer insist that this energy is re-emitted by the same transition $u \to l$. Instead, we consider all permitted decays from level u and randomly assign the absorbed energy to *one* of these decay channels in accordance with their relative effective emissivities. This is accomplished as follows:

By construction, the permitted decays from level u form a contiguous subset in line list B. If the transition $u \to i$ is the kth member of this subset and $4\pi j_k$ denotes its effective emissivity – i.e. after correcting for photon trapping – then the fraction of the energy emitted by level u that escapes via the kth branch is

$$q_k = j_k / \sum j_m \qquad (8)$$

Accordingly, in deciding to which of the transitions $u \to i$ the absorbed energy should be allocated, we first generate z, a random number from $(0, 1)$, and then compute the sequence of partial sums

$$S_k = \sum_1^k q_m \qquad (9)$$

$k = 1, 2, \ldots$ until the condition $S_k \geq z$ is satisfied. The transition k that first fulfils this inequality is the transition which carries off the absorbed energy and which therefore defines the rest frequency of the photons in the emitted packet. If during the Monte Carlo experiment many excitations to level u occur, then the ensemble of packets assigned randomly to decay channels $u \to i$ in this way will clearly constitute an accurate realisation of the emission from level u.

By avoiding photon splitting, this treatment of branching leads to relatively simple and compact code. The prior computation of line list B also contributes considerably to simplicity and efficiency.

4.2. Line absorption rate

In the procedures described in Papers I and II, a line absorption $l \to u$ results in a packet's entire energy ϵ being absorbed. Accordingly, the obvious estimate for the rate per unit volume at which energy is removed from the radiation field by excitations $l \to u$ is

$$\dot{E}_{lu} = \frac{\epsilon_0}{\Delta t} \frac{1}{V} \sum \frac{\epsilon}{\epsilon_0} \qquad (10)$$

where the summation extends *only* over the packets that are actually absorbed by the transition $l \rightarrow u$ in volume element V. In particular, therefore, packets that are redshifted across co-moving frequency ν_{ul} without suffering absorption make no contribution.

Interestingly, an estimator of higher statistical accuracy can be readily constructed. A photon redshifted into resonance with the line at ν_{ul} has probability $1 - e^{-\tau_{lu}}$ of being absorbed, where τ_{lu} is the Sobolev optical depth. Applying this probability to packets as they come into resonance, we derive the modified estimator

$$\dot{E}_{lu} = \frac{\epsilon_0}{\Delta t} \frac{1}{V} (1 - e^{-\tau_{lu}}) \sum \frac{\epsilon}{\epsilon_0} \qquad (11)$$

where now the summation extends over *all* packets in V whose co-moving frequencies $= \nu_{ul}$ at some time during the Monte Carlo experiment.

For a line with $\tau_{lu} << 1$, it may well happen that no packet is absorbed in V by the transition $l \rightarrow u$. Eq. (10) then gives $\dot{E}_{lu} = 0$ in V, an outcome that is a typical consequence of the limited dynamical range of Monte Carlo simulations. In contrast, in this same circumstance, Eq. (11) correctly returns a non-zero value, provided only that at least one packet came into resonance with ν_{ul} in V during the simulation. Given the typical velocity widths of the spherical shells that constitute the discrete volume elements of the SN envelope, this latter, weaker condition is satisfied (except in far UV) if $N \gtrsim 10^3$, a condition fulfilled by a wide margin in routine simulations with the previous code.

4.3. Scaling

At the conclusion of a Monte Carlo simulation, a fraction of the N incident packets are found to have escaped to infinity, and these yield the following estimate of the SN's luminosity,

$$L_{bol} = \frac{\epsilon_0}{\Delta t} \sum_{\infty} \frac{\epsilon}{\epsilon_0} \qquad (12)$$

But since we choose to regard L_{bol} as an input parameter, this estimator in fact serves to fix the scaling constant $\epsilon_0/\Delta t$, and this then allows all other estimators to be converted to physical units.

In Sect. 2, the option of taking $L(\lambda_1, \lambda_2)$ as luminosity parameter was mentioned. In this case, the summation in Eq. (12) is restricted to escaping packets in (λ_1, λ_2) and then $\epsilon_0/\Delta t$ fixed as before.

With $\epsilon_0/\Delta t$ thus determined, the value of T_b is updated from the equation

$$L^+(R) = N \frac{\epsilon_0}{\Delta t} = 4\pi R^2 \sigma T_b^4 \qquad (13)$$

which derives from Eq. (1). Note that, for this simple model, iterations are required only to determine T_b since it in turn determines T_R and T_e and therefore also the stratification of excitation and ionization.

4.4. Relativistic terms

In Paper II, it was shown how easily relativistic terms (except for time delay) can be incorporated into a Monte Carlo treatment of radiative transfer. However, an essential element of this investigation is the application of Sobolev theory to Monte Carlo simulations, and the formulation of Sobolev theory used (Lucy 1971) neglects all terms of $O(v/c)$ except for the Doppler effect. Accordingly, for consistency, this same level of approximation is used here also in the Monte Carlo Calculations.

Note that the neglect of relativistic terms only introduces errors of $\lesssim 10\%$, substantially less than the likely uncertainties in the density profile, in the stratification of abundances, and in the ionization balance.

5. Emergent spectrum

In this section, a procedure for calculating the emergent spectrum is developed that is greatly superior to the crude estimate provided by the frequency distribution of escaping packets. This procedure uses the formal integral for the emergent intensity but with line and continuum source functions derived from the Monte Carlo experiment.

5.1. Basic idea

Without recourse to Monte Carlo techniques, noise-free SNe spectra can be computed by incorporating Sobolev theory into a formal integral calculation of the luminosity density L_ν (e.g. Lucy 1991). However, this requires that the source functions be known or, equivalently, the level populations. Accordingly, in the context of a NLTE treatment of level populations, the formal integral approach is indeed preferable to a Monte Carlo simulation. However, in the context of approximate treatments of level populations and line formation, the relevance of the formal integral is not at all evident. Nevertheless, the prospect of thereby eliminating or reducing sampling errors makes this approach worth exploring.

One obvious possibility would be to eliminate the Monte Carlo calculation entirely and simply compute the emergent spectrum from the formal integral with source functions evaluated using our approximate formulae (Sect. 2) for the level populations. However, the resulting emergent spectrum would differ systematically from the corresponding Monte Carlo spectrum. Moreover, apart from sampling errors, the Monte Carlo spectrum will in general be closer to the truth than the formal integral spectrum calculated in this way.

To justify this latter remark, suppose that, for some ion, our approximate formulae seriously overpopulate a normal level u. In the above hypothetical formal integral calculation, this error directly translates into enhanced emissivities for all lines $u \rightarrow l$, with corresponding spurious emission bumps in the emergent spectrum. On the other hand, in the Monte Carlo simulation, emission in the transitions $u \rightarrow l$ only arises following absorptions that excite level u, and these occur at a rate governed by the typically much more reliably estimated populations of the ground state and other low-lying (especially metastable) levels.

With the origin of this expected superiority of the Monte Carlo spectrum thus understood, it is now of interest to construct a formal integral procedure that incorporates this highly desirable insensitivity to the population of upper levels. To do this, the line source functions implicit in the Monte Carlo simulation must be extracted. This in turn can be done by noting that, in effect, the Monte Carlo simulation derives line emissivities for transitions $u \to l$ by applying approximate branching ratios q_{ul} to the rate at which transitions $l \to u$ absorb energy.

5.2. Line source function

Expressed in terms of level population and Einstein coefficients, the general expression for the line source function is

$$S_{ul} = \frac{A_{ul} n_u}{B_{lu} n_l - B_{ul} n_u} \tag{14}$$

and this is the form useful in a formal integral calculation after a NLTE determination of the level populations.

Because a NLTE calculation is not carried out, it is useful first to express the line source function in terms of the line's effective emissivity, which, in the Sobolev approximation, is

$$4\pi j_{ul} = A_{ul} n_u h\nu_{ul} \beta_{ul} \tag{15}$$

where

$$\beta = \frac{1}{\tau}(1 - e^{-\tau}) \tag{16}$$

is the escape probability and

$$\tau_{lu} = h\nu_{ul}(B_{lu} n_l - B_{ul} n_u)\frac{\lambda_{ul} t}{4\pi} \tag{17}$$

is the Sobolev optical depth. Note that τ is given here in the form appropriate for velocity law $v = r/t$ and that Einstein B-coefficients have been preferred to the oscillator strength and statistical weights.

From Eqs. (14)–(17), it immediately follows that

$$4\pi j_{ul} = \frac{4\pi}{\lambda_{ul} t}(1 - e^{-\tau_{lu}})S_{ul} \tag{18}$$

a formula valid for line formation in a SN envelope treated in the Sobolev approximation.

Eq. (18) now allows the line source function to be computed from data accumulated during the Monte Carlo simulation. The steps are as follows:

1) From the values of $\dot{E}_{lu}$ given by Eq. (11), we immediately have an estimate of the total rate per unit volume at which energy is absorbed in exciting level u,

$$\dot{E}_u = \sum_{i<u} \dot{E}_{iu} \tag{19}$$

Moreover, from the discussion in Sect. 4.2, we expect this estimate to be superior to that obtained simply by tallying absorbed packets.

2) For the adopted model of line formation, the fraction q_{ul} of this absorbed energy escapes via the branch $u \to l$. Accordingly, the effective line emissivity is estimated to be

$$4\pi j_{ul} = q_{ul} \dot{E}_u \tag{20}$$

Note that the Sobolev optical depths and escape probabilities needed to evaluate these branching probabilities from Eqs. (8) and (15) are derived using our approximate formulae for excitation and ionization (Sect. 2).

3) Finally, substitution of this value of $4\pi j_{ul}$ into Eq. (18) gives the desired line source function S_{ul}.

From the discussion in Sect. 4.2 of the superior performance expected of the estimator for $\dot{E}_{lu}$ given in Eq. (11), it follows that the above steps for extracting S_{ul} from a Monte Carlo simulation should yield data from which a high quality emergent spectrum can be derived. In particular, thousands of weak lines in a typical line list, the majority of which neither absorb nor emit a packet during a simulation, will be assigned non-zero values of S_{ul} by this procedure.

5.3. Continuum source function

In addition to bound-bound transitions, our model of a SN's reversing layer also includes electron scattering. This process must therefore also be included in the formal integral calculation, and so the corresponding source function, the mean intensity in the co-moving frame, must be derived. Fortunately, this quantity is readily evaluated at the many thousands of frequencies in a typical line list by applying Sobolev theory to the estimates of $\dot{E}_{lu}$ given by Eq. (12).

If J_{lu}^b denotes the co-moving mean intensity of the incident radiation in the far blue wing of the transition $l \to u$, then the mean intensity of the partially attenuated incident radiation averaged over the line profile is, in the Sobolev approximation, $\beta_{lu} J_{lu}^b$. Accordingly, the rate at which this transition absorbs energy from the incident radiation field is

$$\dot{E}_{lu} = (B_{lu} n_l - B_{ul} n_u)\beta_{lu} J_{lu}^b h\nu_{ul} \tag{21}$$

When combined with Eqs. (14) and (15), this implies that

$$\dot{E}_{lu} = \frac{4\pi}{\lambda_{ul}}(1 - e^{-\tau_{lu}})J_{lu}^b \tag{22}$$

a formula that allows J_{lu}^b to be derived from the values of $\dot{E}_{lu}$ given by Eq. (12). Note that an implicit assumption here is that there are no population inversions so that stimulated emissions can be treated as negative absorptions and τ_{lu} remains non-negative. The excitation formulae of Sect. 2 are consistent with this assumption.

From the values of J_{lu}^b so derived, the corresponding quantity in the extreme red wing, J_{lu}^r, can also be derived with a further application of Sobolev theory. Applying the analysis in Lucy (1971) to velocity law $v = r/t$, we readily find that

$$J_{lu}^r = J_{lu}^b e^{-\tau_{lu}} + S_{ul}(1 - e^{-\tau_{lu}}) \tag{23}$$

Accordingly, with J_{lu}^b and S_{ul} already derived from $\dot{E}_{lu}$, this equation gives us the further quantity J_{lu}^r. Thus, for each spherical shell of the discretized SN envelope, this analysis gives us

mean intensities in the blue and red wings of every line in the line list, with non-zero values whenever at least one packet came into resonance with the line during the simulation. In Sect. 5.5, these discrete values of J_ν are used to approximate the electron scattering source function.

5.4. Monte Carlo estimator for J^b_{lu}

From Eqs. (12) and (22), we immediately derive

$$J^b_{lu} = \frac{\lambda_{ul} t}{4\pi} \frac{\epsilon_0}{\Delta t} \frac{1}{V} \sum \frac{\epsilon}{\epsilon_0} \qquad (24)$$

as a Monte Carlo estimator for the mean intensity in a line's extreme blue wing, where, as for Eq. (12), the summation is over packets that resonate with the line during the simulation.

In the original version of this investigation, this formula was derived from an energy density argument (cf. Lucy 1999) and was the starting point for the source function calculations developed in this Section. Here preference has been given to the $\dot{E}_{lu}$ estimator as starting point because the origin of superior performance is then clearer. Nevertheless, it is worth emphasizing that this estimator for J^b_{lu} provides the radiative coefficients for a NLTE treatment of excitation carried out in the context of a Monte Carlo simulation. Moreover, in accordance with the discussion of Sect. 4.2, these coefficients are non-zero provided only that at least one packet comes into resonance during the simulation: it is not actually necessary that any excitations $l \to u$ occur.

5.5. Formal integral

If $I_\nu(p)$ denotes the limiting specific intensity at rest frequency ν of a beam that intersects the SN envelope with impact parameter p, then

$$L_\nu = 8\pi^2 \int_0^\infty I_\nu(p) p\, dp \qquad (25)$$

is the luminosity density in the rest frame.

To calculate $I_\nu(p)$, we must evaluate (i) the increments in intensity due to line formation at the points where the beam resonates with lines and (ii) the increments due to electron scattering along the segments between consecutive resonances. If ν_k denotes the line frequencies in line list A, then the line formation increment at the point of resonance with ν_k is given by Sobolev theory as

$$I^r_k = I^b_k e^{-\tau_k} + S_k (1 - e^{-\tau_k}) \qquad (26)$$

where the superscripts r and b denote the far red and blue wings as before, and S_k is derived as described in Sect. 5.2.

Now, in the absence of continuum processes, we would have $I^b_{k+1} = I^r_k$ as in Lucy (1991), and so we could proceed recursively through the line list to calculate the limiting intensity. But here electron scattering is included, and we estimate its contribution over the segment between the k and $(k+1)$th resonances as

$$I^b_{k+1} = I^r_k + \Delta\tau_e (J_{k,k+1} - I^r_k) \qquad (27)$$

where $\Delta\tau_e (\ll 1)$ is the electron scattering optical depth along that segment, and $J_{k,k+1}$ denotes the average co-moving mean intensity along the same segment. For this latter quantity, we adopt the approximation

$$J_{k,k+1} = \frac{1}{2}(J^r_k + J^b_{k+1}) \qquad (28)$$

with the quantities on the right-hand-side calculated as described in Sect. 5.3.

The initial conditions required for the recursive application of Eqs. (26) and (27) are: I^b_1 if $p > R$ and $I^b_m = B_\nu(T_b)$ if $p < R$, where m denotes the first transition in line list A for which the point of resonance is above but not occulted by the lower boundary $r = R$.

6. Numerical results

In this section, the validity of the innovations developed in Sects. 4 and 5 are investigated. In addition, some implications of the revised treatment of line formation are illustrated.

6.1. Line formation

In order to construct a test of the revised treatment of line formation, we first consider the NLTE populations of an ion's discrete levels in the low density limit. With no contribution to line emissivity from collisional excitation and no energy exchange with the radiation field due to photoionizations or recombinations, the solution of the equation of statistical equilibrium is such that the ion is in thermal equilibrium with the radiation field. Specifically, in the stated circumstances, statistical equilibrium implies that

$$\sum_u \sum_{l<u} 4\pi j_{ul} = \sum_u \sum_{l<u} \dot{E}_{lu} \qquad (29)$$

where $4\pi j_{ul}$ and $\dot{E}_{lu}$ are given by Eqs. (15) and (21).

We can now interpret the treatments of line formation as schemes to impose this condition of ionic thermal equilibrium when computing the radiation field even though the NLTE populations are not solved for. Thus, with the previous code's assumption of resonance scattering, the line emissivity is

$$4\pi j_{ul} = \dot{E}_{lu} \qquad (30)$$

and so Eq. (29) is enforced by taking each transition to be in thermal equilibrium with the radiation field. On the other hand, with the inclusion of branching in the revised code, the line emissivity is (Sect. 5.2)

$$4\pi j_{ul} = q_{ul} \sum_{i<u} \dot{E}_{iu} \qquad (31)$$

which, when summed over l, gives

$$\sum_{l<u} 4\pi j_{ul} = \sum_{l<u} \dot{E}_{lu} \qquad (32)$$

Accordingly, in this case, Eq. (29) is enforced by means of this thermal equilibrium condition on excitations to and deexcitation from each level u.
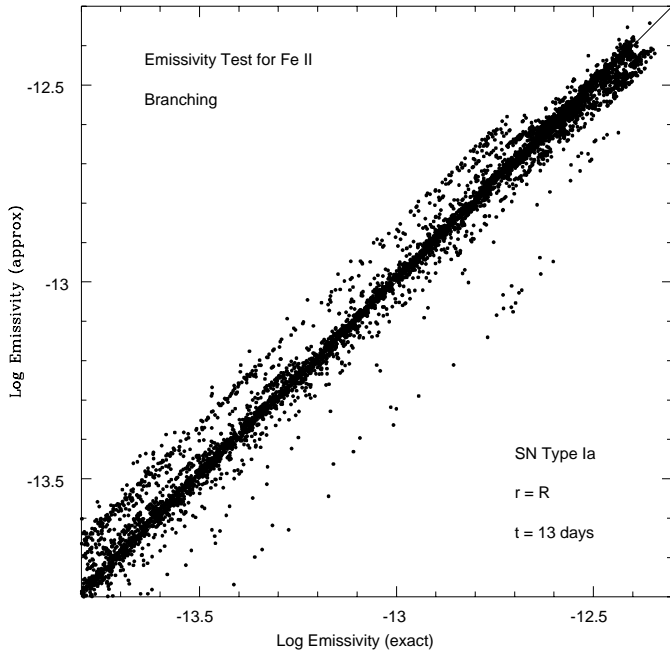
Fig. 1. Effective line emissivities predicted by branching model plotted against exact values for Fe II lines formed at r = R for the Type Ia SN test case. The units of emissivity are $\mathrm{erg\,s^{-1}\,cm^{-3}}$.

Fig. 2. Same as Fig. 1 but for line formation by resonance scattering.

Fig. 3. Same as Fig. 1 but at r = 2R.

This interpretation of line formation models suggests that they be tested by solving the NLTE discrete-level problem for some ion in the low density limit and then comparing the approximate emissivities predicted by Eqs. (30) and (31) with the exact values given by Eq. (15).

This test has been carried out on a 394-level atomic model of Fe II at various radii in our Ia model at $t = 13$ days with $v_{ph} = 11000\,\mathrm{km\,s^{-1}}$. The mean intensity J_{nu} incident at the blue wings of the Fe II transition is taken to be $WB_\nu(T_b)$ with $T_b = 12500\,K$. But even with J_ν known, this NLTE problem is non-linear because the escape probabilities β depend on the unknown level populations. Fortunately, simple repeated back substitutions yield an accurate solution in ~ 5–10 iterations.

In Fig. 1, the emissivities predicted by the branching model at the photosphere $(r = R)$ are plotted against the exact values for lines within a factor ~ 30 of the strongest line. Gratifyingly, we see that numerous lines indeed have $j_{approx} \simeq j_{exact}$, and these form a dense ridge in this plot. Nevertheless, there is a sprinkling of outliers with errors up to 0.4 dex. Overall, for the entire list of 12,302 permitted lines, the emissivity-weighted absolute error is 5.5%.

For comparison, Fig. 2 repeats the above but with the previous code's assumption of resonance scattering. The number of outliers is noticeably increased, as are their errors. The corresponding weighted error is 9.1%.

Since effective line formation continues far out in a SN's atmosphere, the calculation of Fig. 1 has been repeated at $r = 2R$. The result as shown in Fig. 3 is a sharp improvement in the precision of the approximate emissivities, as is in fact to be expected for a model that is asymptotically exact as $W \to 0$. The weighted error in this case is 1.5%.
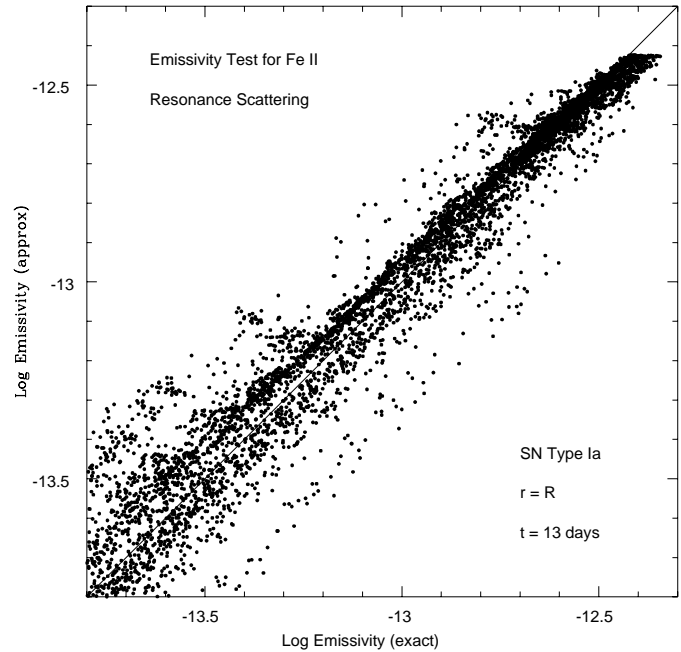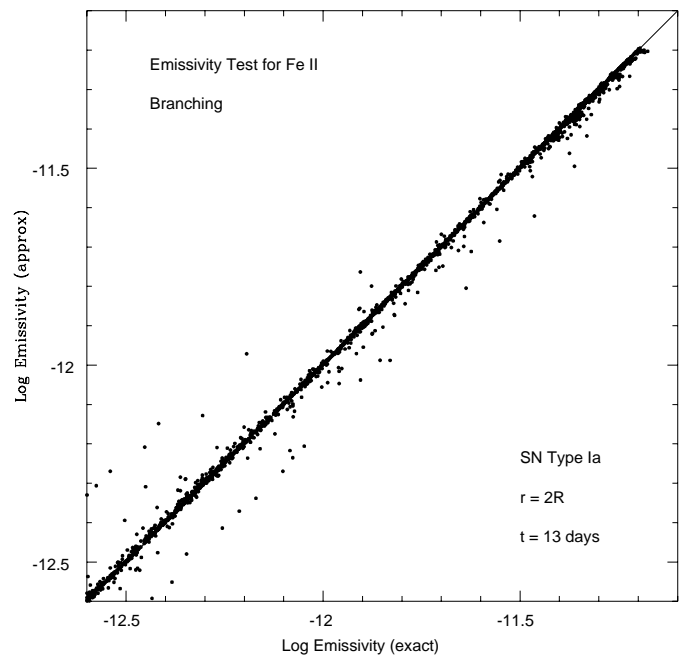
This test of the branching model for this important ion confirms the expected improvement over the resonance-scattering model and indicates that a satisfactory level of accuracy has been achieved. Nevertheless, this test also confirms the earlier remark (Sect. 1) that treating all permitted transitions as resonance scatterers is more accurate than one might intuitively expect. Accordingly, although this improvement is certainly welcome, diagnostic analyses made with the previous code should not be regarded as discredited.
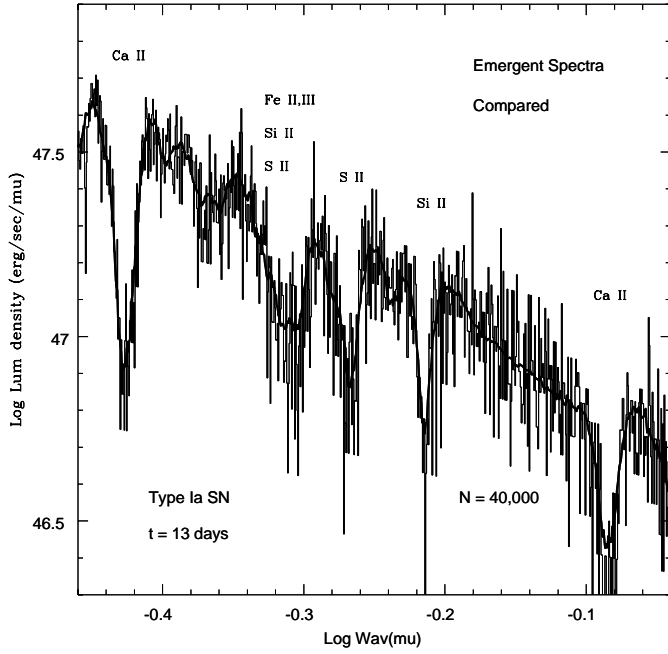
Fig. 4. Monte Carlo and Formal Integral spectra in the optical – near IR for the Type Ia SN test case from a simulation with N = 40,000 packets. The dominant contributors to the absorption troughs are indicated.

Fig. 5. L_λ-weighted percentage errors of Monte Carlo (open circles) and Formal Integral (filled circles) as a function of simulation size N. Least-squares fits of Eq. (34) are also plotted.

By rigorously reradiating absorbed energy, our treatment of line formation implicitly assumes negligible creation or destruction of photons by electron collisions. This can be checked for Fe II by comparing the emissivities computed for Ne = 0 with those for Ne corresponding to all species being singly ionized. The resulting weighted errors of the Ne = 0 emissivities are 2.6% at r = R and 0.01% at r = 2R. The neglect of collisions is therefore justified at maximum light.

It should perhaps be emphasized that, in an actual simulation, the emissivities will be less accurate than shown here due to errors in the level populations. What these tests indicate is the contribution of the line formation approximation to the error budget.

6.2. Emergent spectrum

To illustrate and investigate the computation of SNe spectra by applying the formal integral approach to Monte Carlo simulations as described in Sect. 5, the following parameters are selected: $t = 13$ days, $\log L/L_\odot = 9.44$, and $v_{ph} = 11,000 \, \mathrm{km \, s^{-1}}$. Iterations for the boundary temperature then give $T_b \simeq 12500 \, K$. Accordingly, this quantity is now also regarded as known, and all simulations reported here use this value. By thus fixing T_b, the only quantities varying from simulation to simulation are the seed for the random number generator and N, the number of packets.

As a first step, the optical – near IR spectra given by the two computational procedures for this test case are plotted together in Fig. 4. In this simulation, $N = 40,000$ and the constant velocity width of the spectral bins is $386 \, \mathrm{km \, s^{-1}}$. For the Monte Carlo (MC) spectrum, these choices result in such large sam-

pling errors that the predicted spectrum is close to useless for analysing an observed spectrum. On the other hand, from the same simulation, the formal integral (FI) spectrum shows little evidence of sampling errors and would seem eminently suitable for comparison with real spectra. Moreover, to the eye, the FI spectrum is not inconsistent with our expectation for the MC spectrum from a much larger simulation. This strongly suggests that, in computing the FI spectrum, we have in effect greatly accelerated the convergence of the Monte Carlo procedure.

To investigate this accelerated convergence quantitatively, a sequence of simulations for this test case has been carried out with N increasing from 10^4 to 10^7. From this sequence, the FI spectrum for $N = 10^7$ is taken to be 'exact' – i.e., to be identical with L_λ^∞, the MC spectrum in the limit $N \to \infty$. With this assumption, we can estimate the L_λ-weighted absolute errors

$$\delta = \sum | L_\lambda - L_\lambda^\infty | / \sum L_\lambda^\infty \qquad (33)$$

of the other spectra in the sequence.

In Fig. 5, the percentage errors given by this formula are plotted against N for both the MC and FI spectra. From this plot, we see that the 'errors' of the MC spectra decrease as N increases, consistent with our assumption that the FI spectrum for $N = 10^7$ does not differ markedly from the MC spectrum in the limit $N \to \infty$.

With this point thus experimentally confirmed, the data in Fig. 5 now allows us to assess the degree of accelerated convergence achieved. To this end, the plotted logarithmic errors have been fitted by least squares to the functional form

$$\delta = \delta_0 \left(\frac{10^4}{N} \right)^{1/2} \qquad (34)$$

The resulting scaling constants are $\delta_0 = 2.87\%$ for the FI spectra and $\delta_0 = 51.3\%$ for the MC spectra. These fits are plotted in Fig. 5 and seen to represent the data well.

From these values of δ_o or directly from Fig. 5, we see that, for the chosen binning, the typical error of a point on the MC spectrum is a factor ~ 18 larger than for the FI spectrum. More importantly, to achieve some specified precision, the MC spectrum requires a simulation with a factor ~ 320 increase in N compared to that for the FI spectrum. This huge acceleration of convergence obviously translates rather directly into reduced computer time per spectrum; and this allows the spectra from numerous models to be used in the analysis of a single observed spectrum.

In the above convergence test, the noisy MC spectra were not smoothed. The question therefore arises of whether the huge convergence gain survives if the sampling fluctuations are smoothed. Accordingly, the test has been repeated with the MC spectra smoothed by the method of fourth differences (Lanczos 1956). The result is that δ_o for the MC spectra decreases to 37.9% and the convergence gain factor drops to ~ 170. Evidently, the FI spectra provide a genuinely huge gain in computational efficiency.

It is informative also to apply this same smoothing operation to the FI spectra. We first note that if an approximate theoretical spectrum is not subject to sampling errors, then smoothing will in general worsen its fit to the exact spectrum. This is in fact what happens with the FI spectra. All the FI spectra in the above sequence are degraded by smoothing, and this becomes a marked effect as $N \to \infty$. For example, for $N = 1.3 \times 10^6$ an FI spectrum with $\delta = 0.28\%$ is degraded to 0.73% by smoothing. This experiment confirms the negligible impact of sampling errors on the FI spectra when $N \stackrel{>}{\sim} 10^4$.

Although highly successful, these tests do indicate that some aspects of the procedures in Sect. 5 warrant improvement. In Fig. 5, the δ's for the MC spectra trend above the $N^{-1/2}$ fit for large N, and this is confirmed by two independent sequences of simulations. This suggests a slight difference $\sim 2\%$ between the MC and FI spectra in the limit $N \to \infty$. Given the other uncertainties in the computation of SNe spectra, this slight discrepancy is not of immediate concern.

6.3. Implications

An option included in the present code is that of disallowing branching and thereby reverting to resonance scattering. The implications of branching can therefore be investigated with all other aspects fixed.

With identical stratification of ionization and excitation thus ensured, simulations for these two line formation mechanisms have the same Sobolev optical depths for all transitions at all points in the envelope. Accordingly, the absorption components of P Cygni line profiles are identical if formed against the continuum emitted by the lower boundary. But even in this case, the emission components will in general differ since the branching code does not, for each transition, impose numerical balance between absorbed and emitted packets.
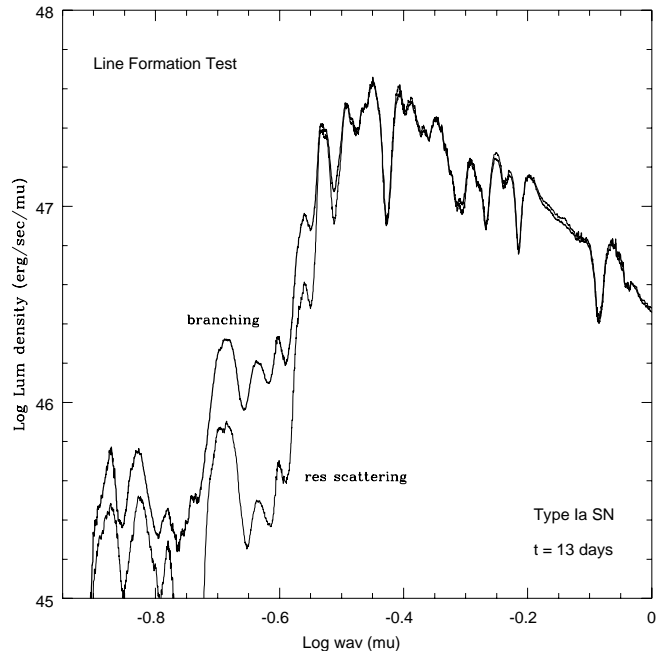
Fig. 6. Formal integral spectra for Type Ia SN test case with line formation by branching (bold line) and resonance scattering (thin line).

The cumulative differential effect of branching on the emergent spectrum is illustrated in Fig. 6, where spectra for our test case for each mechanism are superposed. The differences in the optical – near IR are evidently inconsequential. However, at $\lambda \stackrel{<}{\sim} 2800$A, the fluxes predicted with branching are 0.2–0.6 dex higher than with resonance scattering. Now, with the latter mechanism, UV fluxes are low due to severe line blocking by thousands of metal lines. But with branching, these low fluxes are enhanced by the addition of an emission-line spectrum due to radiation diverted from *longer* wavelengths. This *reverse* fluorescence effect results from the absorption of optical radiation by an ion in an initial excited state (usually metastable) followed by decay to a final state of lower energy. The ions responsible for this effect in order of importance are Fe II, Fe III and Ni II.

The inconsequential changes in the optical revealed by Fig. 6 would at first seem to imply that resonance-line scattering was already of sufficient accuracy for interpreting observed spectra at these wavelengths. However, the enhanced ambient UV radiation field due to this reverse fluorescence effect changes the stratification of temperature, ionization and excitation when the refinements of Paper II are implemented. The resulting changes in Sobolev optical depths then constitute a feedback effect that branching has on the diagnostically-important absorption troughs that dominate optical spectra. The implication of such changes for diagnostic investigations of observed spectra will be discussed in detail by Mazzali (1999).

7. Conclusions

The purpose of this paper has been to describe and test two potential improvements to a Monte Carlo spectral synthesis code

for SNe. To this end, these have been implemented for a simple, test-bed model for the atmosphere of a Type Ia SN.

The first modification replaces the previous code's treatment of all transitions as resonance lines with a treatment of branching based on Sobolev escape probabilities. Interestingly, this improvement in the mechanism of line formation can be incorporated into a Monte Carlo code without introducing photon splitting, thus avoiding the coding complexity that such splitting surely entails.

In support of this upgrade, a quantitative test of the intrinsic precision of the branching model carried out for the crucial Fe II ion demonstrates a satisfactory overall accuracy as well as a useful gain in accuracy relative to the resonance-scattering model. Accordingly, the severe redistribution in frequency that radiation suffers in a Type Ia envelope is undoubtedly more accurately treated in the updated code.

The second modification replaces the noisy emergent spectrum obtained by binning escaping packets with a calculation based on the formal integral for emergent intensity. To achieve this, Sobolev theory is used to extract line- and continuum source functions from a Monte Carlo simulation; and this step allows an intervention with theory that dramatically improves the accuracy of line source functions. Because of this latter improvement, the resulting emergent spectra suffer little from sampling errors and demonstrably achieve an accuracy that with simple binning would require a simulation larger by a factor ~ 320. This huge gain in computational efficiency greatly enhances the diagnostic power of the updated code, since in future numerous theoretical spectra can be generated as one adjusts parameters and varies the stratification of elements in the attempt to fit an observed spectrum.

The code described in this paper is the prototype for a new spectral synthesis code for future use in rapidly carrying out coarse spectral analyses for newly-discovered SNe. To this end, this code together with the atomic data files I and II derived from the Kurucz-Bell (1995) data have been transferred to P.A. Mazzali for the incorporation of the refinements of Paper II. In a companion paper (Mazzali 1999), he will describe this further step as well as discussing the diagnostic implications of the modifications.

References

Abbott D.C., 1982, ApJ 259, 282

Abbott D.C., Lucy L.B., 1985, ApJ 288, 679

Branch D., Doggett J.B., Thielemann F.-K., 1985, ApJ 294, 619

Chugai N.N., 1980, Sov. Astr. Letters 6, 266

Eastman R.G., Pinto P.A., 1993, ApJ 412, 731

Fosbury R.A.E., Danziger I.J., Lucy L.B., Gouiffes C., Cristiani S., 1987, In: Danziger I.J. (ed.) ESO Workshop on SN 1987A

Kurucz R.L., Peytremann, 1975, Smithsonian Astrophysical Observatory Special Report 362

Kurucz R.L., Bell B., 1995, Kurucz CD-ROM No. 23

Lanczos C., 1956, Applied Analysis, Prentice Hall, Englewood Cliffs N.J., 316

Lucy L.B., 1971, ApJ 163, 95

Lucy L.B., 1987a, In: Danziger I.J. (ed.) ESO Workshop on SN 1987A, p. 417 (Paper I)

Lucy L.B., 1987b, A&A 182, L31

Lucy L.B., 1991, ApJ 383, 308

Lucy L.B., 1999, A&A, in press

Mazzali P.A., Lucy L.B., Butler K., 1992, A&A 258, 399

Mazzali P.A., Lucy L.B., 1993, A&A 279, 447 (Paper II)

Mazzali P.A., Lucy L.B., Danziger I.J., et al., 1993, A&A 269, 423

Mazzali P.A., Danziger I.J., Turatto M., 1995, A&A 297, 509

Mazzali P.A., Chugai N., Turatto M., et al., 1997, MNRAS 284, 151

Mazzali P.A., 1999, in preparation

Nomoto K., Thielemann F.-K., Yokoi K., 1984, ApJ 286, 644

Patat F., Benetti S., Cappellaro E., et al., 1996, MNRAS 278, 111

Schmutz W., Abbott D.C., Russell R.S., Hamann W.-R., Wessolowski U., 1990, ApJ 355, 255

Strömgren B., 1939, ApJ 89, 526

Zhang Q., Hu J.Y., Wang L.F., Mazzali P.A., Wang Z.R., 1995, MNRAS 277, 1115